A quantum-mechanical investigation of oxygen vacancies and copper doping in the orthorhombic CaSnO3 perovskite

Oxygen Vacancy and Copper Doping in the Orthorhombic $CaSnO_3$ Perovskite: A DFT Study

J. Maul,[1,2,3,*] I. M. G. Santos,[2] J. R. Sambrano,[3] S. Casassa,[1] and A. Erba[1]

[1] *Dipartimento di Chimica, Università degli studi di Torino, Via Giuria 5, 10125 Torino, Italy*
[2] *Núcleo de Pesquisa e Extensão: Laboratório de Combustíveis e Materiais, Universidade Federal da Paraíba, CEP 58051-900, João Pessoa, PB, Brazil*
[3] *Computational Simulation Group, CDMF-UNESP, São Paulo State University, CEP 17033-360, Bauru, SP, Brazil*

(Dated: May 18, 2018)

In this study we explore the implications of the oxygen vacancy V_O formation and of copper doping on the orthorhombic $CaSnO_3$ perovskite, by means of density functional theory. We focus on energetic and electronic properties. In particular, the electronic charge distribution is analyzed in terms of Mulliken, Hirshfeld-I, Bader and Wannier approaches. In all cases, the different approaches used to analyze the electron change distribution, provide a consistent picture. Calculations are performed at PBE and PBE0 level (for the doping with Cu only PBE0), with both spin-restricted and spin-unrestricted formulations; unrestricted calculations are used for spin-polarized cases and for the naturally open-shell cases (Cu doping). A supercell (2x2x2) approach is used to avoid interactions among periodically repeated defects. The oxygen vacancy is found to have the tendency to reduce the Sn neighbors by giving rise to an energy band within the energy bang-gap of the pristine system, close to the valence band. At variance with what happens in the $CaTiO_3$ perovskite (also investigated here), the oxygen vacancy in the $CaSnO_3$ perovskite is found to lose the two valence electrons and thus to be positively charged so that no F-center is formed. As regards the Cu doping, when one Sn atom is substituted by a Cu one, the most stable configuration corresponds to having the Cu atom as first neighbor to the vacancy. These findings shed some light on the catalytic and phosphorous host properties of this perovskite.

I. INTRODUCTION

Perovskites, and in particular those belonging to the ABO_3 family, are a class of materials characterized by a large variety of cationic and anionic compositions of great interest in the field of solid state chemistry and physics because of their many possible applications.[1–8] Among them, calcium stannate, $CaSnO_3$, has promising use as phosphorous host,[9–14] component of optoelectronic devices,[15] and as an unconventional luminescent material.[16–18]

Point-defects of ordered materials represent one of the most studied topics in solid state science, given that they can significantly alter several physical and chemical properties of a material. Among those, the oxygen vacancy is clearly one of the most commonly reported point-defects of oxides-based catalysts.[19–28] In particular, a wealth of information on this subject is available for the prototypical TiO_2 catalyst, in which this defect is "easily" formed in its reactive type.[29–31] Doping (i.e. atomic substitution) is another popular source of point-defects that, if properly controlled, can be used to tune some properties of the material.[32–37]

An oxygen vacancy V_O in an ionic material can range between two ideal limits: neutral, $V_O^{\times}$ and doubly positively-charged, $V_O^{\bullet\bullet}$, the neutral one being commonly associated with an F-center (color center) in perovskite structures.[38–40] Three previous theoretical studies addressed the issue of the formation of an oxygen vacancy in the $CaSnO_3$ perovskite. The first study was carried out by Urusov *et al.*[41] and took advantage of a classical description of an ionic lattice. The second one used a high-throughput density functional approach to screen more than 5000 perovskite structures; among them, Emery and Wolverton proposed the stability of orthorhombic $CaSnO_3$ and studied the formation of the oxygen vacancy.[42] The third used DFT calculation of the vacancy concomitant to lanthanum doping to some alkaline earth stannates.[43]

In this study, we characterize the energetic and electronic aspects of the formation of an oxygen vacancy in the $CaSnO_3$ orthorhombic perovskite by using the density functional theory in a generalized-gradient approximation (GGA) and with a hybrid approach, including some non-local exact exchange. We also focus our attention to the Cu-doping given that this element is considered in several studies as a tuning medium for the catalytic activity, particularly so in Sn containing structures.[44–48] Formation energies are computed, the electronic structure of the defect-containing structures analyzed in terms of projected density-of-states and the electron charge distribution of the defects investigated in terms of many different schemes: Mulliken, Hirshfeld-I, Bader and Wannier, which, when combined, provide a rather comprehensive characterization of the defects.

II. METHODOLOGY AND COMPUTATIONAL SETUP

All calculations are performed using the CRYSTAL17 programs.[49,50] We use all-electron atom-

centered Gaussian-type-function (GTF) basis sets, the same already used in our previous studies on this system.[51,52] They are described by a 8(s)6511(sp)21(d), 9(s)763111(sp)631(d) and 6(s)2111(sp)1(d) contraction of primitive GTFs for Ca, Sn and O atoms, respectively. Additionally a 8(s)64111(sp)41(d) all-electron basis set is considered for Copper.[53] The calculations are performed at PBE[54] and PBE0[55] level.

The tolerances for the evaluation of Coulomb and exchange series are set to 7,7,7,7,14 for all calculations.[56] The convergence on energy was set to 10^{-8} Hartree for the optimization procedure using a quasi-Newton optimizer combined to a BFGS algorithm for Hessian updating. The shrinking factor was set to 8 for the bulk (20 atoms/cell) and to 2 for the 2x2x2 supercell (160 atoms/cell) calculations of the $CaSnO_3$ *Pbnm* structure.

To calculate the formation energies of the defects, we also simulate CuO and SnO_2 bulks and the O_2 molecule using the same computational conditions as the ones adopted for the $CaSnO_3$ structure. Charge density integration for Bader analysis was performed adopting the most dense integration grid and including 10 stars of neighbors as possible attractors[57] whereas the default parameters were used in the Hirshfeld-I iterative procedure.[58] Further information on the structural models used is given in subsection II A.

Two different "removal" models are here adopted for the oxygen vacancy formation: the first one is based on the complete removal of the atom and its basis set, hereafter called "atom removed" (AR), the second one involves the removal of the atom mass and charge but maintains its basis set, henceforth to be referred to as "ghost" (GH). We will discuss these two schemes when addressing the point of whether the oxygen vacancy in $CaSnO_3$ is neutral (i.e. possibly giving rise to an F-center) or not. To further check the correctness of our description, both models (AR and GH) are also used to describe the oxygen vacancy in the orthorhombic *Pbnm* $CaTiO_3$ perovskite with the same computational conditions. This is because this latter system is known to present a F-center, as other titanates and zirconates, and thus constitute an excellent benchmark to validate our approach.[59–63]

A. Structural Models for Oxygen Vacancy and Cu Doping in $CaSnO_3$

The primitive cell of the bulk structure of the orthorhombic $CaSnO_3$ perovskite contains 4 formula units (20 atoms/cell). The cell contains two symmetry-independent oxygen atoms: one apical O_{ap} and one equatorial O_{eq}, that represent the two possible independent sites for the formation of the oxygen vacancy V_O. Both oxygen atoms are bridging two tin atoms (Sn–O–Sn). A 2x2x2 symmetrical supercell is built, which contains 160 atoms. At variance with cubic perovskites, the centro-symmetric orthorhombic structure is characterized by only 8 symmetry operators, out of which 6

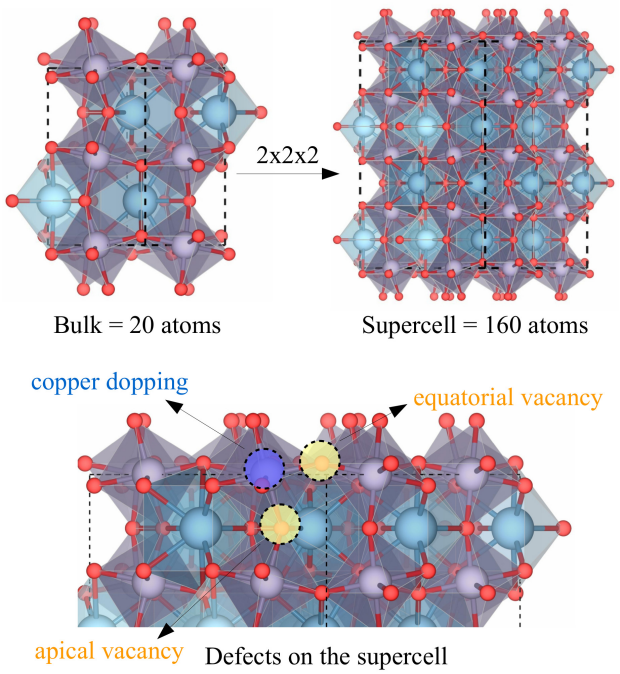

FIG. 1: (color online) Sketch of the structures (bulk and supercell) and defect sites of $CaSnO_3$.[64]

are lost when the supercell is built so that the supercell only exhibits the inversion symmetry. This symmetry loss obviously increases the computational time of the corresponding calculations, and represents one of the reasons why perovskite-type materials have often been studied computationally employing cubic or pseudo-cubic structures.[59,62] When modeling the defects (oxygen vacancy or Cu doping) also the inversion symmetry is lost.

A sketch of the structure and defect sites is given in Figure 1. The position of the apical and equatorial oxygen atoms is showed and the substitution site for copper atom also indicated, which is placed in the octahedral site of SnO_6, thus forming a CuO_6.

The copper doping calculations are performed solely at PBE0 level, since the inclusion of a fraction of exact Fock exchange is crucial to a correct description of spin localization, as also observed in the simple CuO bulk case. We have considered two models for Cu doping: i) the first one is a simple substitution of tin by copper atoms, without further electronic compensation; ii) the second one is a tin-copper substitution in the presence and vicinity of an oxygen vacancy. In the latter case, different structural models are considered with different relative position of the Cu atom and the oxygen vacancy: i) Cu as first neighbor to the vacancy; ii) Cu as second neighbor to the vacancy with a connecting path of the kind Cu—O_{eq}—Sn—V_O; iii) Cu as third neighbor to the vacancy with a connecting path of the kind Cu—O_{ap}—Sn—V_O.

The balanced charge and mass reactions investigated in this study are summarized in Eqs. (1)-(3) according

to Kröger-Vink's notation:

$$\text{null} \xrightarrow{\text{CaSnO}_3} \text{Sn}''_{\text{Sn}} + V^{\bullet\bullet}_{\text{O}} + \frac{1}{2}\text{O}_{2(\text{g})} \quad (1)$$

$$\text{CuO} + \frac{1}{2}\text{O}_{2(\text{g})} \xrightarrow{\text{CaSnO}_3} \text{Cu}''_{\text{Sn}} + 2h^{\bullet} + \text{SnO}_2 \quad (2)$$

$$\text{CuO} \xrightarrow{\text{CaSnO}_3} \text{Cu}''_{\text{Sn}} + V^{\bullet\bullet}_{\text{O}} + \text{SnO}_2 \quad (3)$$

Eq. (1) refers to the oxygen vacancy formation in pristine $CaSnO_3$, which is accompanied by an electronic compensation due to the reduction of a tin ion formally from Sn^{4+} to Sn^{2+}. Eq. (2) refers to the simple substitution of a Sn atom by a Cu atom, compensated by the formation of two electron holes. Finally, Eq.(3) refers to the Cu-doping in the presence of an oxygen vacancy. It is worth pointing out that these are merely charge and mass balanced equations, using classical charge concepts, here displayed for facilitate the discussion.

Let us now briefly discuss some aspects of the electronic state of the various model structures. Pristine $CaSnO_3$ is a closed-shell system. We have studied the oxygen vacancy in three different ways: i) as a closed-shell system with a spin-restricted formulation; ii) as a singlet within a spin-unrestricted formulation; iii) as a triplet within a spin-unrestricted formulation. The most stable electronic configuration for the oxygen vacancy in $CaSnO_3$ is found to correspond to a closed-shell solution. We have studied all models for Cu-doping in terms of a spin-unrestricted formulation and found that the corresponding ground state is a spin-doublet. The spin-contamination of all explored electronic states has also been evaluated.

B. Electron Charge Analysis

As anticipated, the electron change distribution of the system has been investigated according to four different partitioning schemes. Indeed, atomic charges do represent one of the most popular tool for the analysis of electron density. Obviously, the partitioning of the total electron density into atomic contributions is somehow arbitrary and can be performed following different strategies that can be divided into two classes depending on whether they are based on the electron density itself or its molecular orbital representation. The simplest scheme belonging to the second class is the so-called Mulliken partition[65] in which atomic charges q depend on the periodic density P and overlap S matrix representations in the basis of atomic orbitals (AO) $\{\chi_\mu(\mathbf{r})\}$ as follows:

$$q_A = \sum_{\mu\in A}\sum_{\nu}^{M}\sum_{g}^{N} P^g_{\mu\nu}\, S^g_{\mu\nu} \quad (4)$$

where the second and third sums run over the M AOs of the reference cell and the N cells of the system, respectively. The first sum is restricted to the AOs centered on atom A. In the CRYSTAL code there are presently two approaches based on the electron density, $\rho(\mathbf{r})$, namely the Bader's QTAIM scheme[66] (Quantum Theory of Atoms in Molecules) first implemented by Gatti et al.[67] in the TOPOND code and subsequently merged[68] into CRYSTAL and the recently implemented Hirshfeld-I method (HI).[69] QTAIM defines atomic basins, Ω, as those surrounded by zero-flux surfaces and $\rho(\mathbf{r})$ is integrated within these regions to get the atomic charge

$$q_A = \int_\Omega \rho(\mathbf{r}) d\mathbf{r} \quad (5)$$

The stockholder partition by Hirshfeld dissects the system into well-defined atomic fragment and the integration of $\rho(\mathbf{r})$ is weighted according to a general and natural choice that is to share the charge density at each point among several atoms in proportion to their free-atom densities, at the corresponding distance from the nuclei.[70] The Hirshfeld-I method[71] has renewed the interest in the original scheme by eliminating the need of calculating the promolecular densities which are replaced with spherical symmetric weight function, $w_A(\mathbf{r})$, optimized through an iterative procedure. The electronic population assigned to a center A is then obtained as

$$q_A = \int_Q w_A(\mathbf{r})\, \rho(\mathbf{r}) \mathbf{dr} \quad (6)$$

In general, as it is also found for molecules,[72] Mulliken tends to provide charges smaller in absolute value than QTAIM and HI provides intermediate values closer to the Bader ones, an effect that becomes more significant as increasing the size of the AO basis set.

Complementary to these standard analysis, an additional procedure based on the Wannier functions (WF), $\{\omega_s\}$, was adopted and fully exploited. WFs provide a picture alternative to that obtained from the Bloch functions (BF) but perfectly equivalent as both span the same translationally invariant space, e.g., occupied manifold and bands of energy states. Their main advantage is to be quadratically integrable in real space and consequently spatially localized. Each WF, resulting from a unitary transformation of the canonical BF,[73] can be given in terms of the AO basis set as

$$\omega_s(\mathbf{r}) = \sum_{\mu}^{M}\sum_{g}^{N} l^g_{\mu s}\, \chi^g_\mu(\mathbf{r}) \quad (7)$$

A Mulliken analysis can then be performed to obtain the atomic population of the sth WF in the reference zero cell

$$Q_{A,s} = \sum_{\mu\in A}\sum_{\nu}^{M}\sum_{g}^{N} l_{\mu s}\, l^g_{\nu s}\, S^g_{\mu\nu} \quad (8)$$

where the superscript $g = 0$ is omitted considering that each WF is perfectly equivalent to all its periodic images.

The atomic population of atom A can be calculated by summing over all the WFs in the reference cell

$$q_A = \sum_s Q_{A,s} \quad (9)$$

The total electronic population on each WF is normalized to one, $\sum_A^M Q_{A,s} = 1$ and the information contained in $Q_{A,s}$ can be employed to characterize the spatial distribution of the sth WF electrons, by defining the atomic delocalization index λ_s as

$$\lambda_s = \left[\sum_A^M \sum_g^N (Q_{A,s}^g)^2 \right]^{-1} \quad (10)$$

that provides an estimate of the mean number of atoms contributing to a given WF. This index is close to 1 for atomic-like WF and is greater than 1 when the electrons are shared among close-by atoms, in particular in the case of covalent bonds. In addition, the degree of localization of WF can be calculated in terms of the trace of the expectation value of the second order moment tensor

$$\sigma_s^2 = \langle w_s | \mathbf{r}^2 - \langle \mathbf{r}_s \rangle^2 | \omega_s \rangle \quad (11)$$

where σ^2 gives a measure of the spatial spread of each WF around its centroid $\langle \mathbf{r}_s \rangle$ and of the extension of its tails.

All these descriptors will be used to get an insight on the features of the electron charge distribution appearing as the oxygen vacancy is created in the $CaSnO_3$ lattice and coupled with a copper substitutional atom.

III. RESULTS AND DISCUSSION

Let us start by describing the density-of-states (DOS) of the orthorhombic $CaSnO_3$ perovskite, which will prove useful for the discussion to follow. The DOS of pristine $CaSnO_3$ is reported in Figure 2. The contributions to the DOS from the various orbitals can be readily identified as the top of the valence band (VB) is mainly due to oxygen p states and the bottom of the conduction band (CB) to tin s and p states, in agreement with previous accounts.[74–77] The two oxygen types, O_{ap} and O_{eq}, contribute differently to the total DOS because of their different concentration (there are 4 O_{ap} and 8 O_{eq} in the cell). In their study of the $CH_3NH_3SnI_3$ orthorhombic perovskite, Bernal *et al.*[78] observed that relevant information on the oxidation state of Sn ions can be obtained from the analysis of the projected DOS. In particular, the presence of Sn s orbitals near the top of the VB suggests a formal Sn^{2+} reduced state while the presence of Sn s orbitals near the bottom of the CB suggests a formal Sn^{4+} full oxidation state. In our case, for the pristine $CaSnO_3$ perovskite, Sn s states are found at the bottom of the CB thus indicating a formal oxidation state of Sn^{4+}. A comprehensive orbital analysis of pristine $CaSnO_3$ has been performed by Mizogushi *et al.*[74]

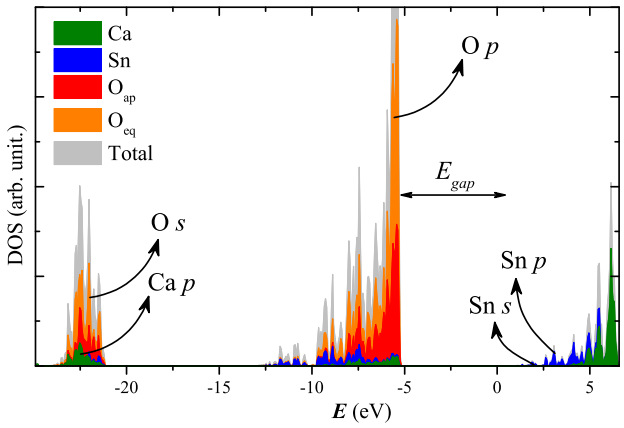

FIG. 2: (color online) Projected density-of-states of pristine $CaSnO_3$.

In the following, we will analyze how the presence of different kinds of defects affects the electronic DOS of the system. In particular, all of the investigated defects introduce new electronic energy levels (and thus some DOS) within the main band gap of the pristine system.

A. The Oxygen Vacancy

1. *Structural Aspects*

The formation of an oxygen vacancy in the $CaSnO_3$ perovskite structure induces a series of structural, and electronic modifications involving chemical bond breaking and rearrangement. Even though these effects propagate over a long range, they are clearly crucial on first and second neighbors. A detailed analysis of the structural changes induced by the formation of an oxygen vacancy, as obtained from full structural relaxations, is presented in Table S1 of the electronic supplementary information (ESI).

First of all, let us discuss the effect that the formation of an oxygen vacancy has on the cell volume. A low defect concentration has been investigated (1 oxygen atom out of 96 has been removed), which is consistent with experimental conditions,[79–82] so that the absolute volume change is small. The specific nature of the electronic state of the defect is found to have a significant impact on the volumetric response: both a closed-shell singlet and a spin-unrestricted singlet states produce a volume contraction while a spin-unrestricted triplet state, where the two unpaired electrons are forced to a spin-up configuration, results in a volume increase. It is also seen that the formation of a vacancy in a O_{eq} site results in a smaller structural deformation than in a O_{ap} site. Indeed, the c crystallographic direction is known to be mechanically softer than the a and b ones, as recently investigated from anisotropic elastic calculations.[51,52] A recent experimental study also confirmed the importance of a detailed di-

rectional analysis for $CaSnO_3$.[83] These structural effects turn out to be rather independent of the particular functional used (GGA or hybrid) as already suggested.[84–87]

2. *Electron Charge Distribution*

As recalled in the introduction, several ABO_3 perovskites exhibit F-centers upon oxygen vacancy formation (i.e. two electrons trapped in the vacancy). In order to check whether or not two electrons are hosted by the vacancy in $CaSnO_3$, we performed an analysis of the electron charge distribution with different approaches. Table S2 of the ESI reports Mulliken and Hirshfeld-I atomic charges for the atoms surrounding the vacancy and the vacancy itself. Despite larger absolute values of the atomic charges obtained from the Hirshfeld-I scheme compared to the Mulliken one, both methods provide the same overall picture and trends. In particular, both approaches describe an "empty" vacancy with no electrons hosted. The electron density analysis performed on the closed-shell state and on the open-shell singlet state provides the same description thus confirming that the ground state of this defect is indeed a closed-shell electronic configuration.

We also performed an analysis of the chemical bond pattern of the defective system based on Wannier functions (i.e. localized valence crystalline orbitals). From this analysis one gets information about where bond orbitals are centered, about what atoms are involved and about what charge they carry. The centroids of the bond Wannier functions around the vacancy are given in Figure S1 of the ESI. None of the obtained valence Wannier bond orbitals is found to involve the atomic functions centered in the middle of the vacancy but one corresponding to a covalent Sn–Sn bond with a tiny electron charge of 0.07 $|e|$ at the center, thus confirming the absence of an F-center. Let us stress that a similar type of bond has also been found for an oxygen vacancy in the inverse spinel $Mg(Mg,Sn)O_4$ structure.[88] The results of the Wannier analysis are found to be independent of the particular functional used and moreover show only little changes from the O_{eq} to the O_{ap} sites. In particular, when the vacancy is formed in a O_{ap} site, the O_{eq} sites become slightly more ionic while the other O_{ap} site remains unchanged. The analysis of the degree of spatial localization of spin-up and spin-down electrons further confirms the higher stability of the singlet electronic state over the triplet one, which would be characterized by a very unbalanced electron distribution.

In order to further corroborate these findings and in particular the presence of a covalent Sn–Sn bond, we have performed a sophisticated topological analysis as proposed by Bader in its quantum theory of atoms in molecules (QTAIM). The analysis is performed with the PBE functional in the GH case. Bader's residual charge on the vacancy is found to be of 0.098 $|e|$ and a bond critical point is found at the mid point between the two

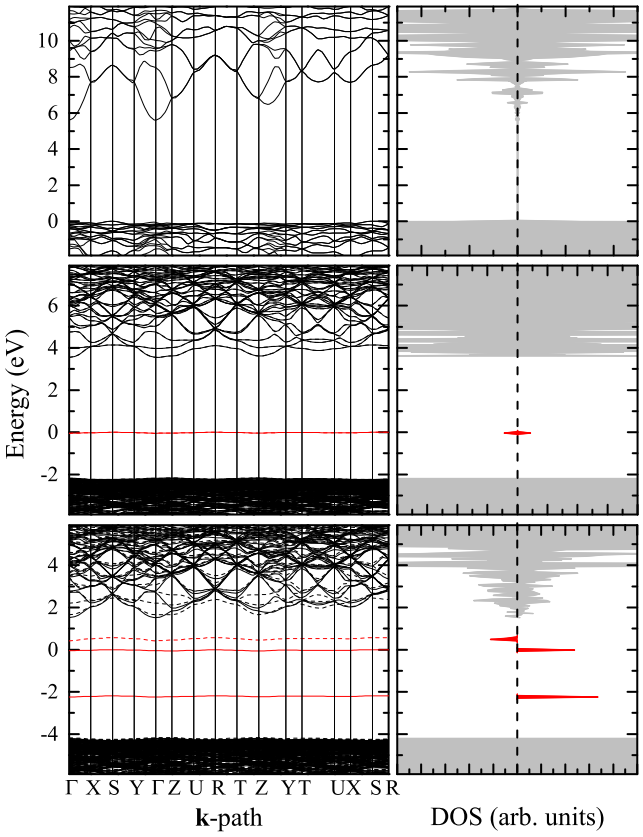

FIG. 3: Electronic band structure (left panels) and density-of-states (right panels) of pristine $CaSnO_3$ (top), and of the defective system with the oxygen vacancy in a singlet (middle) or triplet (bottom) spin configuration. In the DOS representation, spin up and spin down contributions are reported on the right and left of the vertical dashed line, respectively. The electronic states introduced by the defect are reported in red. For each system, the Fermi level is set to zero. Calculations performed with the PBE0 functional.

Sn atoms. According to all the usual descriptors of the QTAIM it is indeed a covalent bond: the Laplacian $\nabla^2\rho$ has a value of -0.008 a.u., the ratio of the potential energy over the positive definite kinetic energy $|V|/G$ of 3.04 and finally the ratio between the total electron energy and the density H/ρ of -0.166 a.u.[89]

The main purpose of the detailed analysis of the electron charge distribution in the defective system was that of checking whether or not an F-center would be formed in the $CaSnO_3$ perovskite upon removal of an oxygen atom. Clearly, the F-center does not arise in this system. Instead of being trapped at the center of the cavity, the two electrons reduce the neighboring Sn atoms, similar to equation (1), and the vacancy is understood as a $V_O^{\bullet\bullet}$ type.[38–40]

3. Electronic Structure

We now analyze the electronic structure of the defective system in terms of band structure and density-of-state. The band structure and the corresponding DOS of the defective system, with the oxygen vacancy in a singlet or triplet spin configuration, are reported in Figure 3 along with those of the pristine system in order to highlight the electronic features introduced by the defect. The electronic states proper to the defect are given in red. The pristine system is characterized by a wide band gap of about 5.6 eV at the PBE0 level of theory. The formation of an oxygen vacancy produces some electronic states with energy levels within the pristine energy band gap. In the singlet spin configuration (the most stable one; see discussion about the energetics in section III A 4), a doubly occupied energy level appears at about 2 eV above the top of the valence band of the pristine system, which reduces the band gap of the system to about 3.6 eV. The band structure of the triplet state is more complex with the formation of three states with energies within the pristine band gap, two occupied by unpaired spin-up electrons and one empty at just 0.5 eV above the highest occupied energy level. In all cases, the defect states are mainly due to s and p orbitals of the two Sn atoms that are first neighbors of the oxygen vacancy. This overall picture is almost independent of the particular site for oxygen substitution and of the way in which the vacancy is described (AR or GH). Furthermore, the same trends are obtained also with the PBE functional (obviously with different absolute values for the band gap).

4. Energetics

The energetics of the formation of an oxygen vacancy in the $CaSnO_3$ perovskite is illustrated in Table I as a function of the different electronic configuration of the defect. The last column of the table reports the electronic band gap E_g where it is seen that the formation of the oxygen vacancy results in a reduction of the pristine band gap by about 2 eV (from 5.6 to 3.6 eV). The triplet electronic state would imply a much lower value of just 0.5 eV as already discussed from the electronic band structures.

TABLE I: Formation energy E_f, relaxation energy E_r, relative configuration energy $E_{\rm conf}$ and electronic energy band gap E_g (all in eV) of the oxygen vacancy in $CaSnO_3$ in different electronic spin configurations (closed-shell CS, singlet S and triplet T). Calculations performed with the PBE0 hybrid functional.

	E_r	$E_{\rm conf}$	E_f	E_g
Pristine	-	-	-	5.6
O Vacancy (CS)	-0.33	0.01	5.23	3.6
O Vacancy (S)	-0.33	-	5.22	3.6
O Vacancy (T)	-0.23	1.80	7.02	0.5

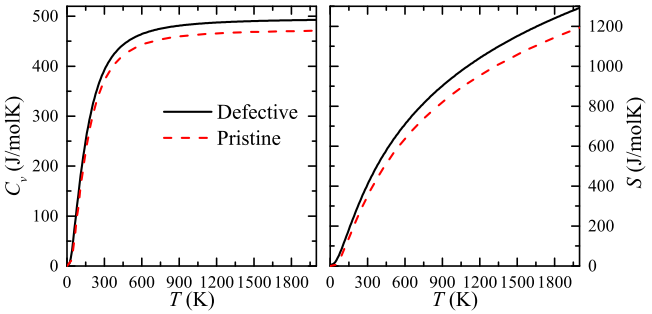

FIG. 4: Constant-volume specific heat (left panel) and entropy (right panel) of the $CaSnO_3$ perovskite without (dashed line) and with the oxygen vacancy (continuous line). The calculation is performed with the PBE functional.

We have computed the formation energy E_f of the oxygen vacancy from the following reaction on our structural model that contains 160 atoms per cell in the pristine system:

$$Ca_{32}Sn_{32}O_{96} \rightarrow Ca_{32}Sn_{32}O_{95} + \frac{1}{2}O_{2(g)} \qquad (12)$$

Three calculations are needed: on the pristine system, on the defective perovskite and on the gas-phase oxygen molecule. From Table I we see that the closed-shell and singlet electronic configurations for the defect are almost energetically equivalent with formation energies of 5.23 and 5.22 eV, respectively. The triplet electronic state corresponds to a much higher formation energy of 7.02 eV, which implies a lower stability of the triplet configuration with respect to the singlet one by 1.8 eV. These values are consistent with those recently reported by Emery and Wolverton.[42] From our calculations, the formation of an oxygen vacancy in an equatorial site is found to be more energetically favored over that in an apical site by about 0.1 eV, which is in agreement with what reported for the $CaZrO_3$ perovskite.[90] Let us stress that, from these static electronic calculations (i.e. performed at 0 K), the formation of the oxygen vacancy would be energetically not favored. We will discuss explicitly the effect of temperature on the formation energy of the defect below.

Table I also reports the relaxation energy E_r defined as the energy gain due to a full structural relaxation upon vacancy creation. This quantity basically quantifies the amount of structural relaxation induced by the formation of the defect. We observe that the structural relaxation is more evident when the defect is in the singlet state; the higher electron-electron repulsion of the triplet configuration indeed does not allow for a relaxation as large as for the singlet configuration. Furthermore, the triplet state is found to be more "spin contaminated" than the singlet one. Indeed, in principle, the electronic

states obtained from unrestricted Kohn-Sham DFT calculations are not guaranteed to be eigenstates of the $\hat{S}^2$ operator. The spin contamination ΔS can be computed as the difference between the actual value of the expectation value of this operator and the ideal expectation value $\Delta S = \langle \hat{S}^2 \rangle - \langle \hat{S}^2 \rangle_{\text{ideal}}$. For singlet and triplet states, $\langle \hat{S}^2 \rangle_{\text{ideal}}$ would be 0 and 2, respectively. No spin contamination is found for the singlet state while a spin contamination of 0.005 is obtained for the triplet state.

5. *Thermodynamics*

In order to take into account thermal effects on the formation energy of the oxygen vacancy in the $CaSnO_3$ perovskite, and, at the same time, in order to check the effect of the vacancy on some thermodynamic properties of the system, we have computed harmonic vibration frequencies of the pristine system and of the defective system for supercells containing 160 (159) atoms. The size of the adopted supercell is such to ensure full convergence of the harmonic thermodynamic properties with respect to the sampling of the phonon dispersion. Given the high computational cost of these calculations, the PBE functional has been used in this case. Figure 4 reports the constant-volume specific heat C_v (left panel) and the vibrational entropy (right panel) as a function of temperature as obtained for the pristine system (dashed lines) and for the defective system (continuous lines). It is seen that the formation of an oxygen vacancy in the $CaSnO_3$ perovskite structure increases its specific heat by about $\Delta C_v = 21$ J/(mol K) in a wide temperature range (from room temperature up to its melting temperature) and increases its vibrational entropy, ΔS, by an amount that increases with temperature. These values are reported in Table II for selected temperatures. In the same table, we also report the computed Gibbs formation free energy of the oxygen vacancy that we have obtained by considering the formation reaction (12) and by working in terms of the Gibbs free energy and no longer in terms of the static purely electronic energy. From the table, it is seen that, as temperature increases, the formation of the oxygen vacancy becomes more energetically favorable. Above about 800 K the formation of the defect becomes spontaneous. For a detailed account on the calculation of defect formation free energies the reader is addressed to Refs. 91 and 92.

TABLE II: Gibbs free energy of formation ΔG_f of the oxygen vacancy in $CaSnO_3$ as a function of temperature. The variation of the constant-volume specific heat ΔC_v and vibrational entropy ΔS of the system due to the vacancy formation are also reported. Thermodynamic properties are obtained from PBE harmonic frequencies.

T (K)	ΔG_f (eV)	ΔC_v [J/(mol K)]	ΔS [J/(mol K)]
0	4.78	-	-
300	3.57	21.38	57.93
600	1.60	21.58	72.80
900	-0.68	21.70	81.58
1200	-3.16	21.75	87.83
1800	-8.53	21.79	96.65

6. *$CaTiO_3$*

As illustrated before, all indicators suggest that no F-center is created in the $CaSnO_3$ perovskite upon formation of an oxygen vacancy: electrons are not trapped in the vacancy but rather reduce the neighboring Sn atoms. On the contrary, an F-center is known to occur in the isostructural orthorhombic $CaTiO_3$ perovskite. In order to check the reliability of our quantum-mechanical calculations, we have also investigated the oxygen vacancy in $CaTiO_3$. In this case, a significant electron density is localized in the vacancy (F-center) and the most stable electronic configuration is the triplet state and no longer the singlet state as in $CaSnO_3$. The energy difference between the AR and the GH description of the vacancy (without and with basis functions centered in the vacancy, respectively) was just 0.2 eV for $CaSnO_3$ while it is 1.11 eV for $CaTiO_3$, that further confirms the need of those functions in the vacancy because of the residual electron density on that site. The electronic band structures of the different spin configurations of the oxygen vacancy in $CaTiO_3$ are reported in the ESI. Moreover, the 3D representation of the spin density of the most stable triplet case is also given in the ESI.

B. Cu Doping

We have already described in Section II A the structural models that we have used to investigate the effect of Cu doping in $CaSnO_3$. In particular, we have studied the substitution of a single Sn atom by a Cu atom (i.e. from SnO_6 to CuO_6) without or with an oxygen vacancy in its spatial vicinity. When the oxygen vacancy and the Cu substitution are both present, different relative distances are considered: the Cu atom can be first, second or third neighbor to the vacancy.

Table S3 of the ESI illustrates the structural changes induced by the Cu doping in the $CaSnO_3$ perovskite with and without oxygen vacancy. The most evident structural change occurring upon substitution is the elongation of the two Cu–O apical bonds in the CuO_6 octahedron, which produce a local distortion towards a planar CuO_4 configuration. The Sn to Cu substitution alone (without oxygen vacancy) results in a decrease of the cell volume. Also the case in which a Cu atom is inserted as first neighbor to the oxygen vacancy results in an overall decrease of the cell volume with respect to the pristine system. However, we observe that when the Cu atom is

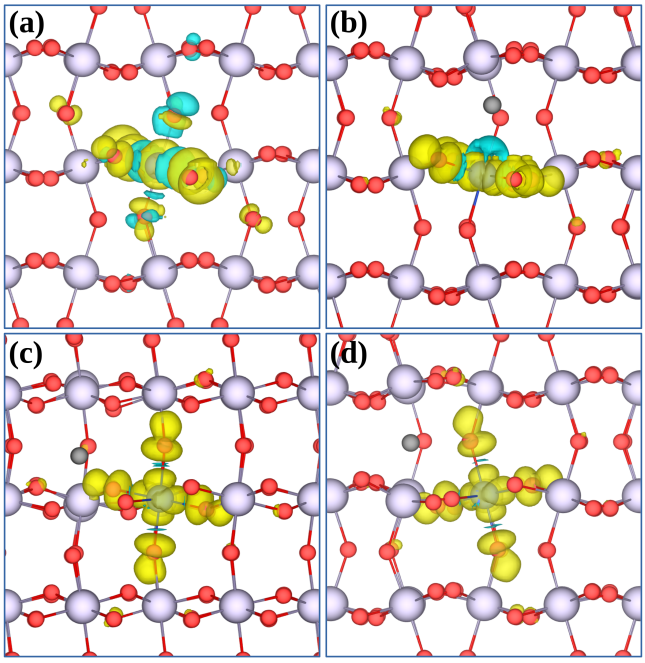

FIG. 5: Spin density 3D maps (cutoff 0.001 e/bohr^3) for (a) the Cu substitution without oxygen vacancy (b) the Cu atom first neighbor to the vacancy (c) the Cu atom second neighbor to the vacancy, and (d) the Cu atom third neighbor to the vacancy. The site of the vacancy is represented as a small dark grey ball. Calculations performed with the PBE0 hybrid functional.

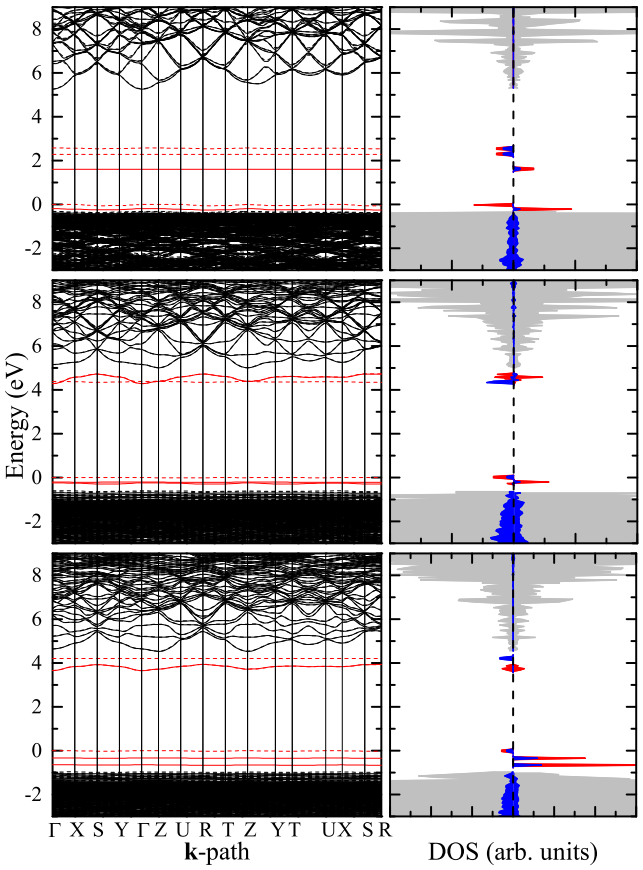

FIG. 6: Electronic band structure (left panels) and density-of-states (right panels) of the Cu doped $CaSnO_3$ perovskite without oxygen vacancy (top), with the oxygen vacancy as first neighbor of the Cu atom (middle) and as second neighbor (bottom). In the DOS representation, spin up and spin down contributions are reported on the right and left of the vertical dashed line, respectively. The electronic states introduced by the defect are reported in red (the contribution of Cu is represented in blue). For each system, the Fermi level is set to zero. Calculations performed with the PBE0 functional.

second or third neighbor to the vacancy the cell volume slightly increases with respect to the pristine system.

The Cu atom is in a d^9 electronic configuration so that it hosts one unpaired electron. Figure 5 reports the spin density of the different models considered for Cu doping and clearly shows that the unpaired electron is always very localized on the Cu and on some of its first neighbors. In particular, the (a) panel corresponds to the case where there is no oxygen vacancy: the unpaired electron is mainly hosted in the CuO_4 plane with some spin density also in the two apical oxygen atoms corresponding to more elongated bonds. Panel (b) shows how a higher spin localization in the CuO_4 plane is achieved when one of the two apical oxygen atoms is removed to form a vacancy (the site of the vacancy is represented as a small dark grey ball). Panels (c) and (d) show the spin localization when the Cu atom is second and third neighbor of the vacancy, respectively. Because of the unpaired electron on the Cu center, all investigated configurations are treated as spin doublets with ideal values of $\langle \hat{S}^2 \rangle_{\text{ideal}} = 0.75$. The highest spin contamination (0.039) is found for the Cu doping case without any oxygen vacancy while the other cases are characterized by a much lower contamination of 0.003, 0.003 and 0.002, respectively.

As observed in the case of the oxygen vacancy alone, also in the presence of Cu doping, the vacancy is found not to host electrons. The Mulliken and Hirshfeld-I analysis of the electron charge distribution for the Cu doping is given in Table S4 of the ESI. We have analyzed the chemical bonding in Cu-substituted $CaSnO_3$ by means of localized Wannier functions and of Bader's QTAIM. Both approaches reveal that, at variance with the case of the oxygen vacancy alone, no metal-metal bond is formed in the presence of a Cu substitution. Not only, no Cu–Sn bond is observed when the Cu atom is a first neighbor of the vacancy, but no Sn–Sn bond is observed when the Cu is second or third neighbor of the vacancy. This confirms that the origin of the covalent Sn–Sn bond when there is the oxygen vacancy alone is due to the induced reduction of the Sn sites close to the vacancy. In the absence of a vacancy, the six Cu–O bonds are found to be more covalent than in the presence of the vacancy. In particular, when the vacancy is a first neighbor to the Cu atom, the four equatorial Cu–O bonds are characterized by a much higher ionicity.

The electronic band structure and corresponding density-of-states of the various configurations of Cu doping here considered are given in Figure 6: the Cu doped $CaSnO_3$ perovskite without oxygen vacancy (top), with the oxygen vacancy as first neighbor of the Cu atom (middle) and as second neighbor (bottom). It is seen that, in all cases, the Sn substitution for Cu creates some electronic states whose energy falls within the pristine gap. This is particularly so when no oxygen vacancy is present. Copper states at the top of the valence band are formed as well as states within the pristine gap, which overall result in a small electronic energy gap of just 1.8 eV (compared to the gap of 5.6 eV of the pristine system). When the Cu atom is first or second neighbor to the oxygen vacancy, the electronic structure is affected differently: some extra density-of-states builds up near the top of the valence band (mainly arising from p oxygen orbitals and d_{z^2} and d_{xy} copper orbitals) and near the bottom of the conduction band (mainly arising from d_{xy} copper orbitals and s and p tin orbitals), resulting in a smaller reduction of the band gap to 4.2 and 3.6 eV, respectively. The presence of copper d states within the pristine gap is relevant to potential catalytic applications.[93–96] The values of the electronic energy band gap E_g of the different configurations of Cu doping are given in Table III.

The energetics of the different doping configurations is given in Table III. The relaxation energy E_r tells us that the smallest structural relaxation occurs when the Cu substitution is done without any oxygen vacancy. When a neighboring oxygen vacancy is present, the structure undergoes a larger structural relaxation as the relative distance of the Cu center and the vacancy increases. This is due to the fact that when the Cu atom is first neighbor to the vacancy the metal-metal covalent bond is not formed. We have also evaluated the formation energy E_f of the different defects. The reaction used to compute the formation energy of the simple Sn for Cu substitution is:

$$Ca_{32}Sn_{32}O_{96} + CuO + \frac{1}{2}O_{2(g)} \rightarrow Ca_{32}Sn_{31}Cu_1O_{96} + SnO_2$$

while the reaction considered for the simultaneous Cu substitution and oxygen vacancy creation is:

$$Ca_{32}Sn_{32}O_{96} + CuO \rightarrow Ca_{32}Sn_{31}CuO_{95} + SnO_2$$

TABLE III: Formation energy E_f, relaxation energy E_r, relative configuration energy $E_{\rm conf}$ and electronic energy band gap E_g (all in eV) of the Sn for Cu substitution in $CaSnO_3$ without and with a neighboring oxygen vacancy. Calculations performed with the PBE0 hybrid functional.

	E_r	$E_{\rm conf}$	E_f	E_g
Pristine	-	-	-	5.6
Cu (no vacancy)	-0.47	-	3.33	1.8
Cu (first neighbor)	-2.17	-	3.01	4.2
Cu (second neighbor)	-2.31	1.45	4.46	3.6
Cu (third neighbor)	-2.42	1.43	4.44	3.7

Energetically, the most stable defect configuration is represented by an oxygen vacancy first neighbor of the Cu atom, which confirms the tendency of defects with opposite local charges to associate.[97–99]

IV. CONCLUSIONS

We have performed density functional theory (DFT) calculations on large structural models to investigate the structural, electronic, energetic, thermodynamic properties of two point-defects in the $CaSnO_3$ perovskite. Hybrid functionals of the DFT have been used, which by including a fraction of exact non-local Fock exchange allow for a reliable description of spin polarized systems.

At variance with what is observed in other ABO_3 perovskites (and notably in $CaTiO_3$), no F-center is created upon formation of an oxygen vacancy in $CaSnO_3$. The two electrons are not "trapped" into the vacancy but rather reduce the neighboring Sn atoms. A Sn–Sn covalent bond is formed bridging the oxygen vacancy. The most stable electronic configuration of the oxygen vacancy defect in $CaSnO_3$ is a singlet, while the triplet polarized state is higher in energy by about 1.8 eV. The formation of the oxygen defect is predicted to significantly affect (increase) the specific heat of the system and to become energetically spontaneous above about 800 K.

Upon copper doping (i.e. substitution of an Sn atom by a Cu one in the octahedral site), the local octahedral site symmetry SnO_6 is distorted to induce a planar CuO_4 configuration with two apical elongated Cu–O bonds. The copper substitution is found to largely reduce the electronic band gap of the system (by about 3.8 eV). The combination of the two defects has also been investigated, according to which the configuration in which the oxygen vacancy is a first neighbor of the Cu atom is found to be the most stable one.

Acknowledgments

J.M. acknowledges the Brazilian scholarship program "Ciência sem Fronteiras" (Process Number 248425/2013-7/SWE) and the Center for Scientific Computing of the São Paulo State University (GridUNESP). Furthermore, we are grateful for the programs PROCAD 2013/Proc. 88881.068492/2014-01 and FAPESP (2013/19289-0, 2013/07296-2). We also would like to thank Prof. R. Orlando and Prof. R. Dovesi for their contributions on the early stages of this study and Prof. C. M. Zicovich-Wilson with whom J.M. developed much of this study in early 2016 at the Centro de Investigación en Ciencias, Universidad Autónoma del Estado de Morelos - Mexico.

* Electronic address: jmaul@quimica.ufpb.br

[1] M. A. Peña and J. L. G. Fierro, Chem. Rev. **101**, 1981 (2001).
[2] A. Kubacka, M. Fernández-García, and G. Colón, Chem. Rev. **112**, 1555 (2012).
[3] R. Thalinger, A. K. Opitz, S. Kogler, M. Heggen, D. Stroppa, D. Schmidmair, R. Tappert, J. Fleig, B. Klötzer, and S. Penner, J. Phys. Chem. C **119**, 11739 (2015).
[4] L. An and H. Onishi, ACS Catal. **5**, 3196 (2015).
[5] E. N. Armstrong, K. L. Duncan, and E. D. Wachsman, Phys. Chem. Chem. Phys. **15**, 2298 (2013).
[6] Y. Yang, J. Íñiguez, A.-J. Mao, and L. Bellaiche, Phys. Rev. Lett. **112**, 057202 (2014).
[7] M. Misono, in *Heterogeneous Catalysis of Mixed Oxides Perovskite and Heteropoly Catalysts*, edited by M. Misono (2013), vol. 176 of *Studies in Surface Science and Catalysis*, pp. 67 – 95.
[8] X. Y. Meng, D. Y. Liu, and G. W. Qin, Energy Environ. Sci. pp. – (2018).
[9] K. Ueda and Y. Shimizu, Thin Solid Films **518**, 3063 (2010).
[10] X. Y. Chen, C. Ma, S. P. Bao, and H. Y. Zhang, J. Alloys Compd. **497**, 354 (2010).
[11] T. Nakamura, M. Shima, M. Yasukawa, and K. Ueda, J. Sol-Gel Sci. Technol. **61**, 362 (2012).
[12] J. Zhang, B. Chen, Z. Liang, X. Li, J. Sun, L. Cheng, and H. Zhong, J. Alloy. Compd. **612**, 204 (2014).
[13] S.-D. Kim, K.-S. Hwang, and S. Hwangbo, Electron. Mater. Lett. **9**, 405 (2013).
[14] K. S. Hwang, Y. S. Jeoni, S. Hwangbo, and J. T. Kim, Ceram. Int. **39**, 8555 (2013).
[15] K. Ueda, T. Maeda, K. Nakayashiki, K. Goto, Y. Nakachi, H. Takashima, K. Nomura, K. Kajihara, and H. Hosono, Appl. Phys. Express **1**, 015003 (2008).
[16] Y. Karabulut, M. Ayvacıklı, A. Canimoglu, J. Garcia Guinea, Z. Kotan, E. Ekdal, O. Akyuz, and N. Can, Spectrosc. Lett. **47**, 630 (2014).
[17] V. Orsi Gordo, Y. Tuncer Arslanli, A. Canimoglu, M. Ayvacikli, Y. Galvão Gobato, M. Henini, and N. Can, Appl. Radiat. Isotopes **99**, 69 (2015).
[18] A. Canimoglu, J. Garcia-Guinea, Y. Karabulut, M. Ayvacikli, A. Jorge, and N. Can, Appl. Radiat. Isotopes **99**, 138 (2015).
[19] M. Suzuki and T. Murakami, Solid State Commun. **53**, 691 (1985).
[20] L. Buannic, F. Blanc, D. S. Middlemiss, and C. P. Grey, J. Am. Chem. Soc. **134**, 14483 (2012).
[21] A. M. Ritzmann, A. B. Muñoz-García, M. Pavone, J. A. Keith, and E. A. Carter, Chem. Mat. **25**, 3011 (2013).
[22] A. M. Deml, V. Stevanoviić, A. M. Holder, M. Sanders, R. O'Hayre, and C. B. Musgrave, Chem. Mater. **26**, 6595 (2014).
[23] I. Kagomiya, K. Jimbo, K.-i. Kakimoto, M. Nakayama, and O. Masson, Phys. Chem. Chem. Phys. **16**, 10875 (2014).
[24] H.-Y. Su and K. Sun, J. Mat. Sci. **50**, 1701 (2015).
[25] K. Eom, E. Choi, M. Choi, S. Han, H. Zhou, and J. Lee, J. Phys. Chem. Lett. **8**, 3500 (2017).
[26] A. L. Gavin and G. W. Watson, Phys. Chem. Chem. Phys. **19**, 24636 (2017).
[27] I. Bredeson, L. Zhang, P. R. C. Kent, V. R. Cooper, and H. Xu, Phys. Rev. Materials **2**, 035401 (2018).
[28] M. Asa, G. Vinai, J. L. Hart, C. Autieri, C. Rinaldi, P. Torelli, G. Panaccione, M. L. Taheri, S. Picozzi, and M. Cantoni, Phys. Rev. Materials **2**, 033401 (2018).
[29] L. Zhang, S. Wang, and C. Lu, Anal. Chem. **87**, 7313 (2015).
[30] K. Tang, A. C. Meng, F. Hui, Y. Shi, T. Petach, C. Hitzman, A. L. Koh, D. Goldhaber-Gordon, M. Lanza, and P. C. McIntyre, Nano Lett. **17**, 4390 (2017).
[31] S. Huygh, A. Bogaerts, and E. C. Neyts, J. Phys. Chem. C **120**, 21659 (2016).
[32] J. A. Dawson, H. Chen, and I. Tanaka, J. Phys. Chem. C **118**, 14485 (2014).
[33] A. Zorko, M. Pregelj, H. Luetkens, A.-K. Axelsson, and M. Valant, Phys. Rev. B **89**, 094418 (2014).
[34] N. Kitamura, J. Akola, S. Kohara, K. Fujimoto, and Y. Idemoto, J. Phys. Chem. C **118**, 18846 (2014).
[35] M. Ito, M. Uchida, Y. Kozuka, K. S. Takahashi, and M. Kawasaki, Phys. Rev. B **93**, 045139 (2016).
[36] S. Lee, H. Wang, P. Gopal, J. Shin, H. M. I. Jaim, X. Zhang, S.-Y. Jeong, D. Usanmaz, S. Curtarolo, M. Fornari, et al., Chem. Mater. **29**, 9378 (2017).
[37] S. Sumithra and N. V. Jaya, J. Mater. Sci. Mater. Electron. **29**, 4048 (2018).
[38] D. Gryaznov, S. Baumann, E. A. Kotomin, and R. Merkle, J. Phys. Chem. C **118**, 29542 (2014).
[39] M. M. Kuklja, Y. A. Mastrikov, B. Jansang, and E. A. Kotomin, J. Phys. Chem. C **116**, 18605 (2012).
[40] D. Gryaznov, E. Blokhin, A. Sorokine, E. A. Kotomin, R. A. Evarestov, A. Bussmann-Holder, and J. Maier, J. Phys. Chem. C **117**, 13776 (2013).
[41] V. S. Urusov and E. V. Leonenko, Mineral. J. pp. 3–11 (2012).
[42] A. A. Emery and C. Wolverton, Sci. Data **4**, 170153 (2017).
[43] L. Weston, L. Bjaalie, K. Krishnaswamy, and C. G. Van de Walle, Phys. Rev. B **97**, 054112 (2018).
[44] S. Zhang, P. Zhang, Y. Wang, Y. Ma, J. Zhong, and X. Sun, ACS Appl. Mater. Interfaces **6**, 14975 (2014).
[45] A. Johari, A. Johari, M. C. Bhatnagar, and M. Sharma, J. Nanosci. Nanotechnol. **14**, 5288 (2014).
[46] C. M. Ghimbeu, M. Lumbreras, M. Siadat, R. C. van Landschoot, and J. Schoonman, Sens. Actuator B-Chem. **133**, 694 (2008).
[47] A. D. Garje, A. Inamdar, and R. C. Aiyer, Int. J. Appl. Ceram. Tech. **8**, 691 (2011).
[48] M. J. Fuller and M. E. Warwick, J. Catal. **34**, 445 (1974).
[49] R. Dovesi, R. Orlando, A. Erba, C. M. Zicovich-Wilson, B. Civalleri, S. Casassa, L. Maschio, M. Ferrabone, M. De La Pierre, Ph. D'Arco, et al., Int. J. Quantum Chem. **114**, 1287 (2014).
[50] R. Dovesi, A. Erba, R. Orlando, C. M. Zicovich-Wilson, B. Civalleri, L. Maschio, M. Rérat, S. Casassa, J. Baima, S. Salustro, et al., WIREs Comput. Mol. Sci. p. e1360 (2018).
[51] J. Maul, A. Erba, I. M. G. Santos, J. R. Sambrano, and R. Dovesi, J. Chem. Phys. **142**, 014505 (2015).
[52] J. Maul, I. M. G. Santos, J. R. Sambrano, and A. Erba, Theor. Chem. Acc. **135**, 1 (2016).
[53] K. Doll and N. Harrison, Chemical Physics Letters **317**, 282 (2000), ISSN 0009-2614.

[54] J. P. Perdew, K. Burke, and M. Ernzerhof, Phys. Rev. Lett. **77**, 3865 (1996).
[55] C. Adamo and V. Barone, J. Chem. Phys. **110**, 6158 (1999).
[56] R. Dovesi, V. R. Saunders, C. Roetti, R. Orlando, C. M. Zicovich-Wilson, F. Pascale, B. Civalleri, K. Doll, N. M. Harrison, I. J. Bush, et al., *CRYSTAL14 User's Manual* (2014).
[57] C. Gatti and S. Casassa, *TOPOND-2013 : an electron density topological program for systems periodic in N (N=0-3) dimensions, User's manual*, CNR-CSRSRC, Milano (2013).
[58] R. Dovesi, V. R. Saunders, C. Roetti, R. Orlando, C. M. Zicovich-Wilson, F. Pascale, B. Civalleri, K. Doll, N. M. Harrison, I. J. Bush, et al., *CRYSTAL 2017 User's Manual* (2017).
[59] R. I. Eglitis, E. A. Kotomin, and G. Borstel, Comput. Mater. Sci. **30**, 376 (2004).
[60] P. G. Sundell, M. E. Björketun, and G. Wahnström, Phys. Rev. B **73**, 104112 (2006).
[61] W.-J. Yin, S.-H. Wei, M. M. Al-Jassim, and Y. Yan, Phys. Rev. B **85**, 201201 (2012).
[62] R. I. Eglitis, Int. J. Mod. Phys. B **28**, 1430009 (2014).
[63] T. S. Bjørheim, M. Arrigoni, D. Gryaznov, E. Kotomin, and J. Maier, Phys. Chem. Chem. Phys. **17**, 20765 (2015).
[64] K. Momma and F. Izumi, J. Appl. Crystallogr. **44**, 1272 (2011).
[65] R. S. Mulliken, J. Chem. Phys. **23**, 1841 (1955).
[66] R. F. W. Bader, *Atoms in Molecules - A Quantum Theory* (Oxford University Press, Oxford, UK, 1990).
[67] C. Gatti, V. R. Saunders, and C. Roetti, J. Chem. Phys. **101**, 10686 (1994).
[68] S. Casassa, A. Erba, J. Baima, and R. Orlando, J. Comp. Chem. **36**, 1940 (2015).
[69] C. M. Zicovich-Wilson, M. Hô, A. M. Navarrete-López, and S. Casassa, Theor. Chem. Acc. **135**, 188 (2016).
[70] F. L. Hirshfeld, Theor. Chim. Acta **44**, 129 (1977).
[71] P. B. C., V. Alsenoy, P. W. Ayers, and R. Carbó-Dorca, J. Chem. Phys. **126**, 144111 (2007).
[72] P. Bultinck, C. V. Alsenoy, P. W. Ayers, and R. Carbó-Dorca, J. Chem. Phys. **126**, 144111 (2007).
[73] C. M. Zicovich-Wilson, R. Dovesi, and V. R. Saunders, J. Chem. Phys. **115**, 9708 (2001).
[74] H. Mizoguchi, H. W. Eng, and P. M. Woodward, Inorg. Chem. **43**, 1667 (2004).
[75] J. M. Henriques, E. W. S. Caetano, V. N. Freire, J. A. P. da Costa, and E. L. Albuquerque, J. Phys.: Condens. Matter **19**, 106214 (2007).
[76] W. Zhang, J. Tang, and J. Ye, J. Mater. Res. **22**, 1859 (2007).
[77] D. Cherrad, M. Maouche, Maamache, and L. Krache, Physica B **406**, 2714 (2011).
[78] C. Bernal and K. Yang, J. Phys. Chem. C **118**, 24383 (2014).
[79] J. A. M. Van Roosmalen and E. H. P. Cordfunke, J. Solid State Chem. **93**, 212 (1991).
[80] Z. Q. Liu, D. P. Leusink, X. Wang, W. M. Lü, K. Gopinadhan, A. Annadi, Y. L. Zhao, X. H. Huang, S. W. Zeng, Z. Huang, et al., Phys. Rev. Lett. **107**, 146802 (2011).
[81] R.-A. Eichel, Phys. Chem. Chem. Phys. **13**, 368 (2011).
[82] H. Tan, Z. Zhao, W.-B. Zhu, E. N. Coker, B. Li, M. Zheng, W. Yu, H. Fan, and Z. Sun, ACS Appl. Mater. Interfaces **6**, 19184 (2014).
[83] J. D. Baniecki, T. Yamazaki, D. Ricinschi, Q. Van Overmeere, H. Aso, Y. Miyata, H. Yamada, N. Fujimura, R. Maran, T. Anazawa, et al., Sci. Rep. **7**, 41725 (2017).
[84] A. Erba, J. Maul, R. Demichelis, and R. Dovesi, Phys. Chem. Chem. Phys. **17**, 11670 (2015).
[85] A. Erba, J. Maul, M. De La Pierre, and R. Dovesi, J. Chem. Phys. **142**, 204502 (2015).
[86] A. Erba, J. Maul, M. Itou, R. Dovesi, and Y. Sakurai, Phys. Rev. Lett. **115**, 117402 (2015).
[87] A. Erba, J. Maul, and B. Civalleri, Chem. Commun. **52**, 1820 (2016).
[88] G. K. Behrh, M. Isobe, F. Massuyeau, H. Serier-Brault, E. E. Gordon, H.-J. Koo, M.-H. Whangbo, R. Gautier, and S. Jobic, Chem. Mater. **29**, 1069 (2017).
[89] S. Casassa, A. Erba, J. Baima, and R. Orlando, J. Comput. Chem. **36**, 1940 (2015).
[90] S. M. Alay-e Abbas, S. Nazir, S. Cottenier, and A. Shaukat, Sci. Rep. **7**, 8439 (2017).
[91] K. Reuter and M. Scheffler, Phys. Rev. B **65**, 035406 (2001).
[92] U. Aschauer, R. Pfenninger, S. M. Selbach, T. Grande, and N. A. Spaldin, Phys. Rev. B **88**, 054111 (2013).
[93] N. Kumagai, L. Ni, and H. Irie, Chem. Commun. **47**, 1884 (2011).
[94] K. J. Pyper, J. E. Yourey, and B. M. Bartlett, J. Phys. Chem. C **117**, 24726 (2013).
[95] T. Wang, X. Yan, S. Zhao, B. Lin, C. Xue, G. Yang, S. Ding, B. Yang, C. Ma, G. Yang, et al., J. Mater. Chem. A **2**, 15611 (2014).
[96] H. Yaghoubi, Z. Li, Y. Chen, H. T. Ngo, V. R. Bhethanabotla, B. Joseph, S. Ma, R. Schlaf, and A. Takshi, ACS Catal. **5**, 327 (2015).
[97] Y.-M. Chiang, W. D. Kingery, and D. P. Birnie, *Physical Ceramics: Principles for Ceramic Science and Engineering* (John Wiley& Sons Inc., 1996), ISBN 9780471598732.
[98] E. Ebsworth, A. Maddock, and A. Sharpe, *New Pathways in Inorganic Chemistry* (Cambridge University Press, 2011), ISBN 9780521279130.
[99] A. De Vos, K. Lejaeghere, D. E. P. Vanpoucke, J. J. Joos, P. F. Smet, and K. Hemelsoet, Inorg. Chem. **55**, 2402 (2016).